Ceramics International 46 (2020) 23854–23866

Contents lists available at ScienceDirect

Ceramics International

journal homepage: www.elsevier.com/locate/ceramint

Enhanced bi-layer mosaic armor: experiments and simulation

Zhong-Nan Zhao[a,b,c], Bin Han[b,*], Fei-Hao Li[a], Rui Zhang[a], Peng-Bo Su[a], Mao Yang[a], Qi Zhang[b], Qian-Cheng Zhang[a], Tian Jian Lu[c,d,**]

[a] State Key Laboratory for Strength and Vibration of Mechanical Structures, Xi'an Jiaotong University, Xi'an, 710049, PR China
[b] School of Mechanical Engineering, Xi'an Jiaotong University, Xi'an, 710049, PR China
[c] State Key Laboratory of Mechanics and Control of Mechanical Structures, Nanjing University of Aeronautics and Astronautics, Nanjing, 210016, PR China
[d] Nanjing Center for Multifunctional Lightweight Materials and Structures (MLMS), Nanjing University of Aeronautics and Astronautics, Nanjing, 210016, PR China

ARTICLE INFO

Keywords:
Mosaic armor
Honeycomb lattice
Ballistic limit
Penetration
Multi-hit resistance

ABSTRACT

Three different alumina/aluminum bi-layer armors having different striking faces, i.e., monolithic alumina, mosaic alumina, and mosaic alumina enhanced by aluminum honeycomb, were fabricated and tested under the impact of the flat projectile. The ballistic performance of each armor type was also investigated using three-dimensional (3D) finite element (FE) simulations. Upon validating the FE simulation results with experimental measurements, the ballistic limit velocity and failure mechanisms for each type of armor, as well as the influence of ceramic tile size, impact position, border effect, and inter tile gap width were quantified. For the enhanced mosaic armor, the metallic honeycomb lattice performed as a cellular skeleton to confine the ceramic tiles and fragments, leading to enhanced ballistic resistance. Besides, the honeycomb enhanced mosaic armor was also found to have much improved multi-hit ballistic resistance in comparison with monolithic and mosaic alumina. The honeycomb preserved the structural integrity of the mosaic armor so that a high level of residual ballistic resistance remained even after impact. With the extended reliability calculation method, single shot ballistic data were used to estimate the performance of the honeycomb enhanced mosaic armor under multiple projectile impacts.

1. Introduction

Lightweight armors with composite configurations combined the advantages of two or more material properties, and had been widely exploited for the protection of human body and civil/military equipment (e.g., vehicles and helicopters) against projectile impact. Since the early work of Wilkins [1], numerous studies had been devoted to investigating bi-layer composite armor systems consisting of a ceramic strike face and a supporting metallic layer behind. The ceramic facing material initially defeated, deformed and eroded the projectile, while the metallic backing plate absorbed the remaining kinematic energy to further increase the fracture and penetration resistance of the armor [2–8].

Generally, a ceramic/metal bi-layer armor system with a monolithic ceramic striking face could provide better ballistic resistance than either a monolithic ceramic armor or a monolithic metal armor of equal mass. However, brittle fracture usually occurred in the ceramic when subjected to projectile penetration. The cracks could extend fast over the entire surface of the monolithic ceramic sheet. That is, it is difficult for the traditional bi-layer armor system to sustain multiple projectile impacts. Nowadays, for automatic weapons and bursting munitions, the dispersion of impacts on the armor could be described as a uniformly random distribution [9]. Therefore, to retain the protectiveness of the composite armor under multiple projectile impacts, how to minimize the damaged area after each single hit became a critical issue. This was usually addressed by reducing the size of ceramic tiles and assembling the tiles in the form of a mosaic-like arrangement to construct the so-called "mosaic armor" or "patterned armor". The mosaic armor had advantages of the flexibility to complex surfaces, low cost and localizing the damage region for multi-hit protection [10,11]. However, there were several shortcomings:

(i) The interfaces between ceramic tiles were necessary but vulnerable [12]. The expansion of the impacted tile could induce damage on all the adjacent tiles [13,14]. Inserting a filling material into the gaps between the mosaic tiles could not only attenuate the

* Corresponding author.
** Corresponding author. State Key Laboratory of Mechanics and Control of Mechanical Structures, Nanjing University of Aeronautics and Astronautics, Nanjing, 210016, PR China.
E-mail addresses: hanbinghost@xjtu.edu.cn (B. Han), tjlu@nuaa.edu.cn (T.J. Lu).

https://doi.org/10.1016/j.ceramint.2020.06.162
Received 25 May 2020; Received in revised form 11 June 2020; Accepted 15 June 2020
Available online 23 June 2020
0272-8842/

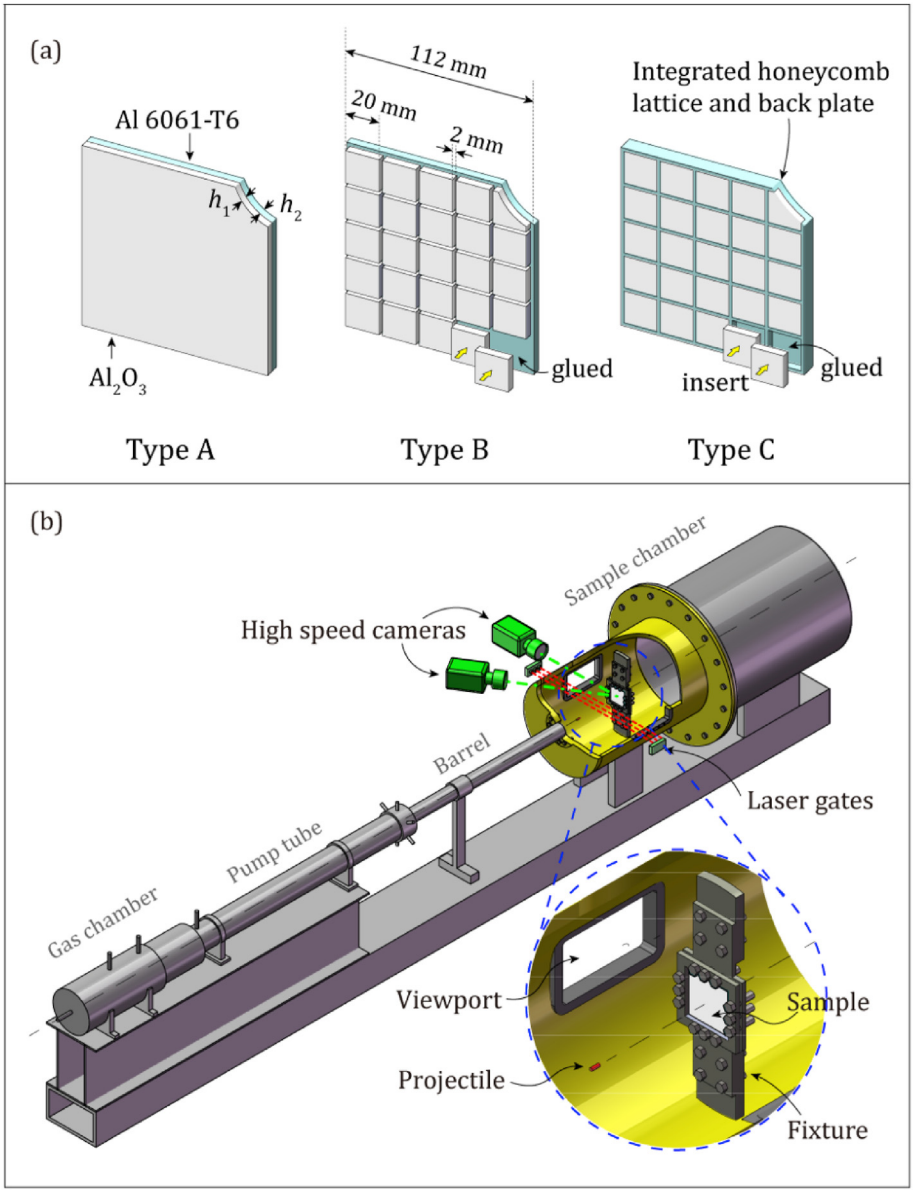

Fig. 1. Schematic of (a) three types of bi-layer armor and (c) ballistic testing system. One corner of the armor was hidden to display its cross-sectional structure.

intensity of stress reflected on the ceramic tile, but also generate a confinement effect on the ceramic tile, thus preventing somehow the fracture of adjacent tiles [15–17].

(ii) The ceramic tiles could not remain bonded to the metallic backing plate during multi-hitting events. Attributed to the deformation mismatch, serious bulging or radial deformation of the backing plate could lead to the detachment of ceramic tiles (adjacent to the one being hit) from the backing plate, which would definitely affect the multi-hit capability of the armor [13,16,18,19].

(iii) The impact position affected the ballistic performance. As for the mosaic armor, the weak zones along the borders of individual tiles and the interfacial gaps among the tiles were both the regions of higher vulnerability of mosaic armor systems [12,20–22].

Although the mosaic armor system had been widely applied in the protection field [13,18,23–25], most existing studies characterized its ballistic resistance only by the performance when the ceramic tile located at the center of the armor was impacted by one single shot. Typically, the mosaic armor exhibited inhomogeneous microstructure, and its ballistic performance and failure mechanisms depended significantly upon the geometric shape and dimensions of ceramic tiles and the impact position. It was therefore not enough to characterize its ballistic performance by considering a single central strike only.

To determine how the ballistic resistance varies with ceramic tile size and evaluate the effect of border proximity, depth of penetration (DOP) tests were performed on a silicon carbide single tile [20]. This study was nonetheless only focused upon a single ceramic tile, that is to say, each tile of a mosaic armor was assumed to perform independently. Also via the DOP tests, the filling material between ceramic tiles in the mosaic armor was found to be beneficial by preventing the expansion of the impacted tile [26]. However, DOP tests with semi-finite backings could not reflect the bonding situation between ceramic tiles and large deformed finite (even thin) back plate in practical applications. Focusing on the influence of inter tile gap width and impacting position, Seifert et al. [21] reported that the ballistic resistance decreased with increasing gap width, and impacting on a ceramic tile located at the edge of the mosaic armor led to the worst ballistic performance. That is, for mosaic armors, the border effect on ballistic resistance is significant. In summary, existing researches seldom compared the ballistic performance of mosaic armor with that of monolithic ceramic armor as well

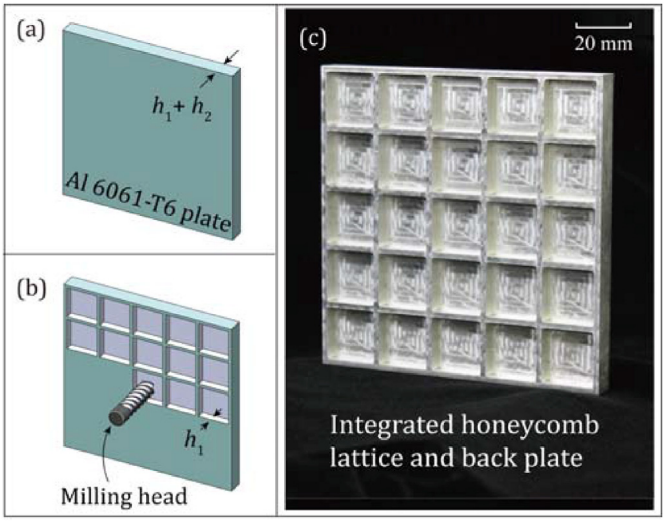

Fig. 2. Fabrication process of the integrated honeycomb lattice and back plate.

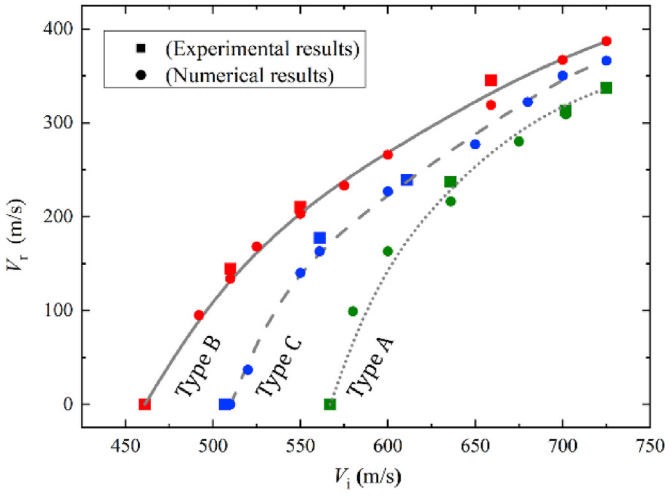

Fig. 3. The residual velocity V_r versus impact velocity V_i for different targets.

as the effects of ceramic tile size, gap width, and impact position. Further, it was necessary to propose an improved design scheme to avoid the inherent shortcomings of current mosaic armor systems.

Metallic lattice truss structures are ultra-lightweight, stiff and strong, and exhibit attractive multifunctional attributes. For instance, hybrid lattice-cored sandwich constructions were envisioned by filling the interstices of corrugated plates or honeycombs with cellular foams, ceramics, sand, concrete and even liquid for enhanced energy absorption and blast/ballistic resistance [27–30]. In the current study, we combined metal honeycomb with mosaic ceramics to construct novel honeycomb enhanced mosaic armor. It was envisioned that, with the metallic honeycomb serving as the cellular skeleton to support and constrain individual ceramic tiles, the shortcomings of traditional mosaic armors as previously detailed could be overcome, in particular the poor multi-hit capability. Cooperated with ceramic tiles of tailored geometrical dimensions, the honeycomb enhanced mosaic armor would be a promising lightweight armor with enhanced ballistic performance.

In the present study, the concept of metallic honeycomb enhanced mosaic armor was proposed, and its ballistic performance was compared with that of traditional mosaic armor using a combined experimental and numerical (finite element) approach. For reference, monolithic ceramic armor was also considered. To explore the mechanisms of a blunt projectile penetrating the armor system, ballistic tests of the three different armors were carried out. Dynamic responses of the ceramic striking face in each armor were captured using high-speed cameras. Three-dimensional finite element models were also established, with the effectiveness of simulation results validated by experimental measurements. The influences of ceramic tile size, impact position, and inter tile gap width on penetration resistance were explored systematically. Finally, single shot ballistic data were used to estimate the performance of enhanced mosaic armor against statistically multiple impacts.

2. Impact tests and characterization

2.1. Bi-layer armor fabrication

Fig. 1a displayed the three different types of ceramic/metal bi-layer armor system considered in the present study:

(A) The baseline alumina/aluminum bi-layer armor. This target comprised a monolithic Al_2O_3 (AD995, density of 3.89 g/cm^3) face plate (i.e., the striking face) and an Al 6061-T6 (yield strength ~324 MPa) back plate. Both the Al_2O_3 face plate and the Al plate were square in shape, each having a width of 112 mm and a thickness of 5 mm. The total thickness of the bi-layer system was 10 mm.

(B) The mosaic armor. Based on Type A, the 5 mm thick Al_2O_3 plate was divided into 25 square tiles with a side length of 20 mm. The inter tile gap width was adjusted by 2 mm thick metal stripes during the bonding process.

(C) The honeycomb enhanced armor. For enhanced ballistic performance, half of a monolithic Al 6061-T6 plate of thickness 10 mm was milled into square honeycomb lattice (Fig. 2), with a web

Table 1
Comparison of ballistic results obtained from simulations and experiments.

Target type	V_i(m/s)	V_r – Experiments(m/s)	V_r – Simulations(m/s)	Error (%)
A	242	0	0	0
	476	0	0	0
	567	0	0	0
	636	237	216	8.86
	702	313	309	1.28
	725	321	337	4.98
B	461	0	0	0
	510	144	134	6.94
	550	210	203	3.33
	659	345	319	7.54
C	389	0	0	0
	507	0	0	0
	561	177	163	7.91
	611	239	229	4.18

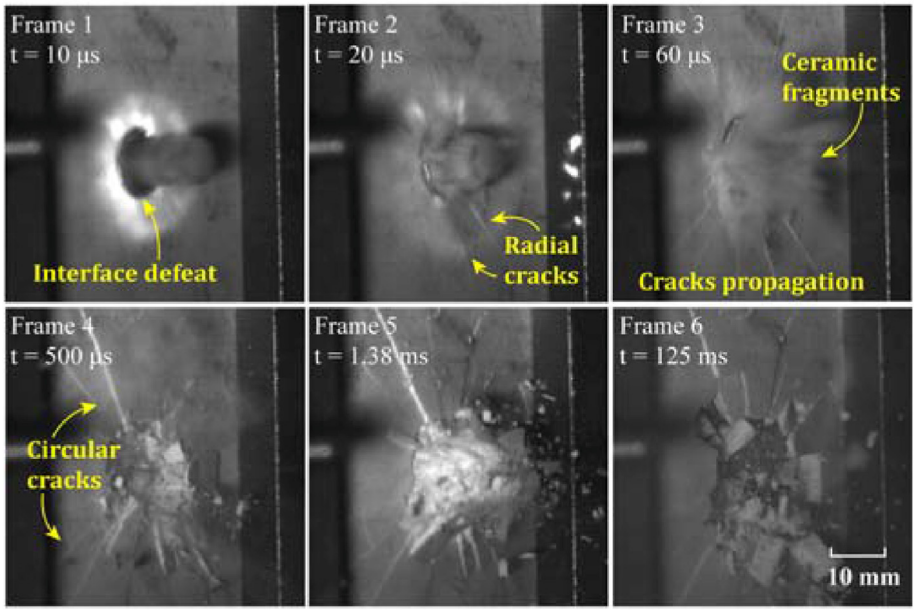

Fig. 4. High-speed image sequence of Type A bi-layer armor impacted at 636 m/s.

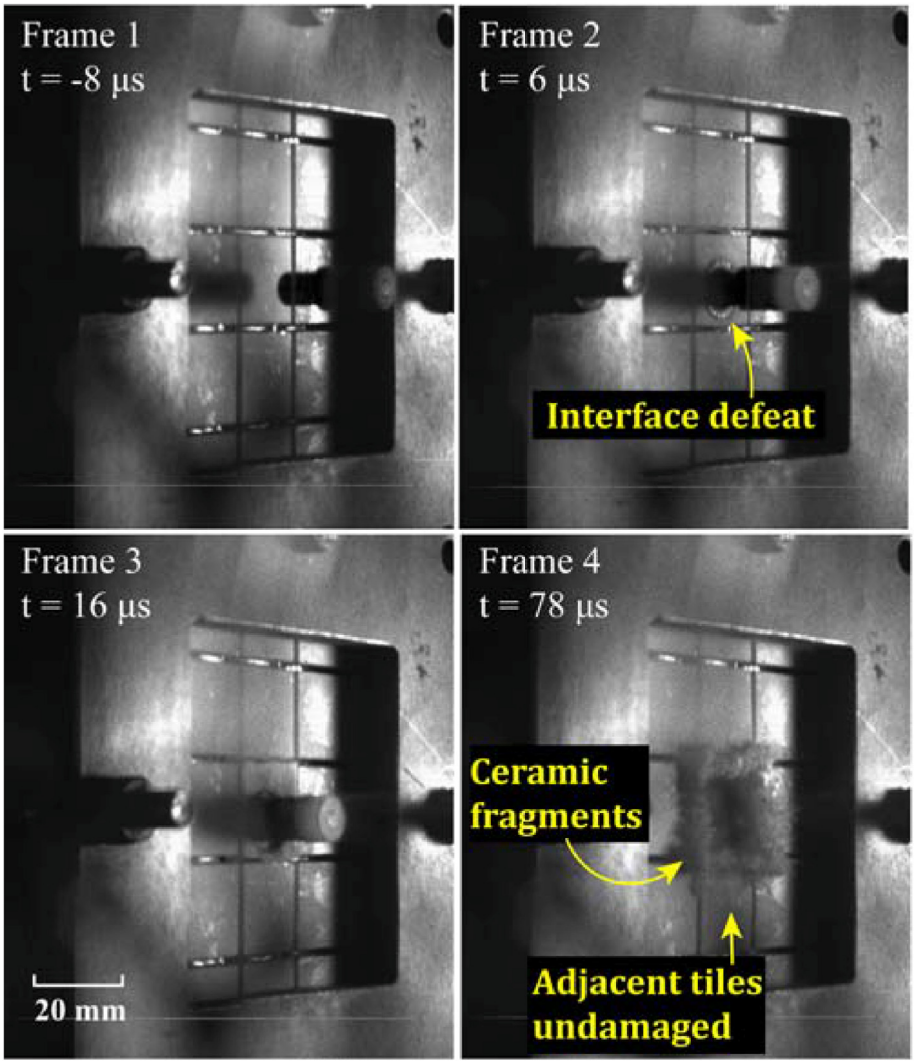

Fig. 5. High-speed image sequence of Type B bi-layer armor impacted at 659 m/s.

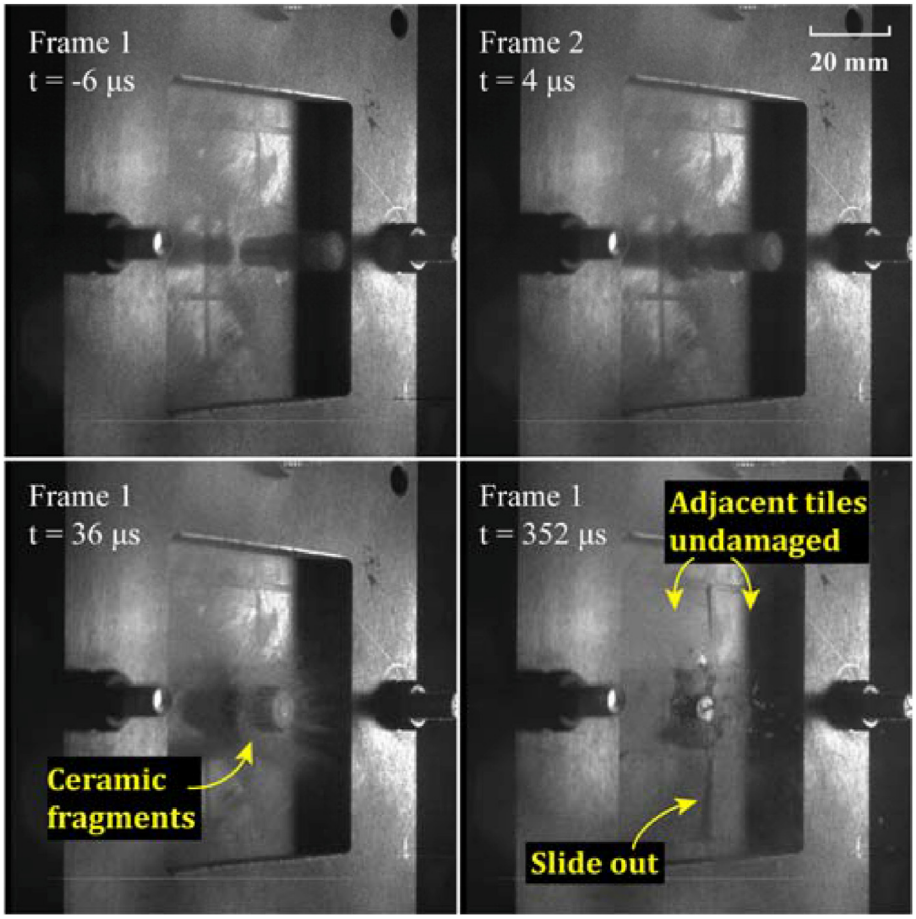

Fig. 6. High-speed image sequence of Type C bi-layer armor impacted at 611 m/s.

thickness of 2 mm. Ceramic tiles, identical to those used in Type B, were subsequently inserted into each cell of the honeycomb (Fig. 1a).

The ceramic was supplied in the form of rectangular tiles with the size of 120 mm × 105 mm × 6 mm. To guarantee a specific inter tile gap, the tiles were cut to the desired dimensions using a diamond wheel, and then the surface was polished by a rough surface grinding wheel, followed by fine grinding. For each armor type, a two-component epoxy adhesive was employed to bond the ceramic tiles to the metal plate, as shown in Fig. 1.

2.2. Impact test protocol

Ballistic tests were performed by using a two-stage light gas gun, as illustrated schematically in Fig. 1b. High purity nitrogen gas was used as the accelerant, and the impact velocity could reach up to 900 m/s. The projectiles were AISI 4340 steel cylinders with diameter (D_p) 7.6 mm, length 20 mm and weight 7.1 g.

The fabricated bi-layer armor with in-plane dimensions of 112 mm × 112 mm were mounted and aligned in a fixture for projectile impact, with 0° obliquity. The sample was positioned so that the impact contact was initiated at the center of its front face (i.e., ceramic). Incident velocities were measured using three laser gates located before the target. The impact position was observed by means of two high-speed cameras to capture the front and rear views of the sample, as shown in Fig. 1b. One camera (Specialised Imaging Inc, Kirana) was employed to monitor the impact side of the ceramic tiles. The other (IX Cameras Ltd, i-SPEED 508) was used to measure the exit velocity of the ejecta, which might consist of ceramic and projectile/target metal fragments.

2.3. Experimental results

The measured impact velocity V_i versus residual projectile velocity V_r responses of three target types investigated were plotted in Fig. 3, with the detailed data as listed in Table 1. In all cases, targets showed a typical ballistic behavior wherein the projectile did not fully penetrate the target up to a critical velocity referred to as the ballistic limit velocity (BLV), i.e. $V_r = 0$ for $V_i <$ BLV. Just above the ballistic limit, the residual velocity of the projectile V_r raised sharply and then increased gradually with the further increase of V_i. The BLV increased in the order: the mosaic ceramic armor (Type B), the honeycomb enhanced armor (Type C) and alumina/aluminum bi-layer armor (Type A).

Figs. 4–6 presented high-speed images of the dynamic deformation and penetration for three types of targets. The moment $t = 0$ corresponded to the instant that the projectile initially impacted the target. For of Type A targets, after impacting on the ceramic striking face, the tip of the projectile started to move radially, leading to the mushroom deformation. During the first microseconds, a stress wave started to propagate from the impact surface of the ceramic tile, resulting in a cracking front advancing in impact direction. This crack front produced two types of cracks, *i.e.*, radial cracks and circular cracks, as shown in Frames 3–4 of Fig. 4. These cracks intersected and extended to all specimen boundaries, resulting in the strength degradation and the final fragmentation of the target. During unloading, lateral cracks formed beneath the impact surface and propagated roughly parallel to it [31]. These cracks intersected radial cracks (frame 4), thereby providing the orthogonal surfaces which led to the formation of fragments. Cratering formed as the fragments splashed from the vicinity of the

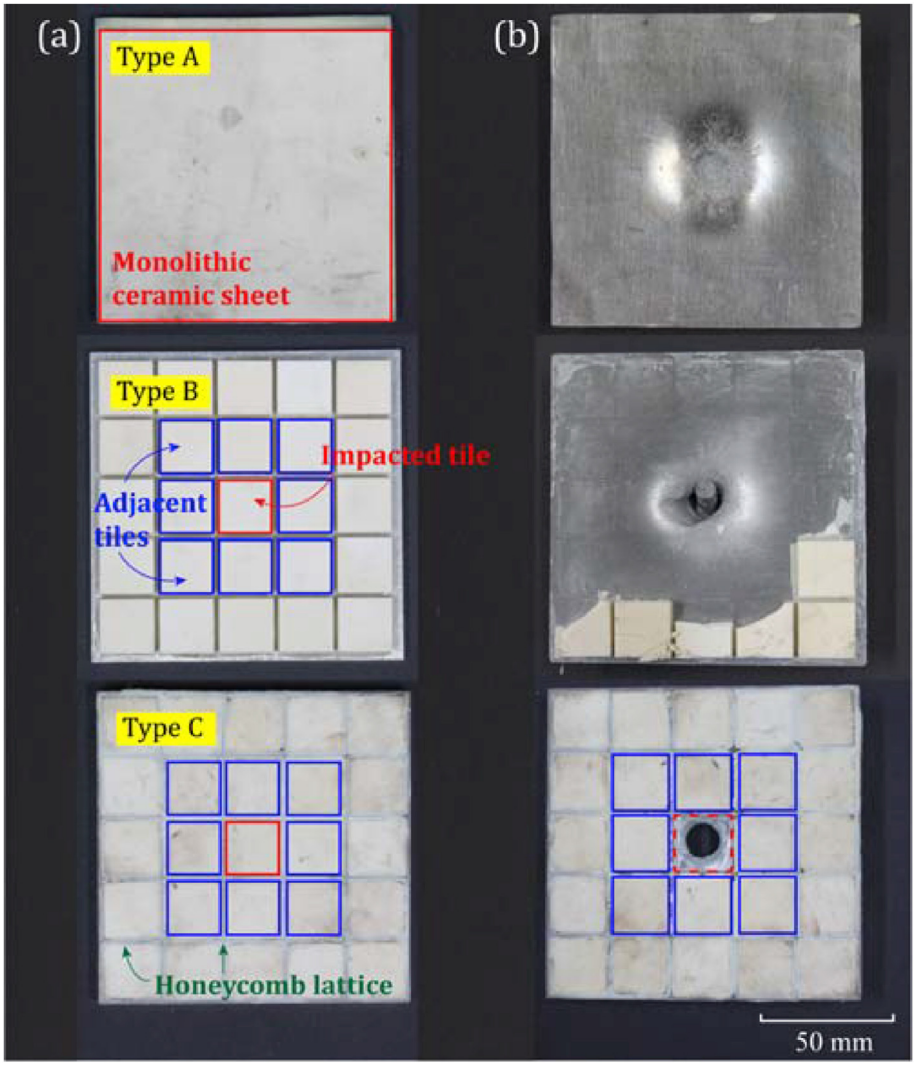

Fig. 7. Photos of three different bi-layer armors (front view): (a) before impact; (b) after impact.

Table 2
Material parameters for AISI 4340 steel [33] and aluminum alloy 6061-T6 [34].

Material/Constants	Steel 4340	Al 6061-T6
Density, ρ (kg/m^3)	7.83	2.7
Shear modulus, G (GPa)	77	27.6
Bulk modulus, K_1 (GPa)	159	27.6
Static yield strength, A (GPa)	0.785	0.324
Strain hardening constant, B (GPa)	0.510	0.114
Strain hardening exponent, n	0.260	0.42
Strain rate constant, C	0.014	0.002
Thermal softening exponent, m	1.03	1.34
Reference strain rate, $\dot{\varepsilon}_0$ (s^{-1})	1793	893
Melting temperature, t_m (K)	477	885

Table 3
Material parameters for AD995 alumina [32].

Material/Constants	Value
Density, ρ (kg/m^3)	3.89
Shear modulus, G (GPa)	152
Pressure constant, K_1 (GPa)	231
Pressure constant, K_2 (GPa)	−160
Pressure constant, K_3 (GPa)	2774
Bulking factor, β	1.0
Hugoniot elastic limit, HEL (GPa)	6.57
Intact strength constant, A	0.88
Intact strength constant, n	0.64
Strain rate constant, C	0.07
Fracture strength constant, B (GPa)	0.260
Fracture strength constant, m	1.0
Hydrostatic tensile limit, T (GPa)	0.312
Damage constant, D_1	0.01
Damage constant, D_2	0.7

impact region.

In the cases of Type B and C targets, radial cracks were arrested by the inter tile gap or honeycomb web, and the damage was confined to the ceramic tile beneath the projectile. For Type B targets, due to the existence of inter tile gaps, the fragments of the ceramic were strongly displaced while adjacent tiles were not affected, which led to the worst performance. For Type C targets, the honeycomb lattice could not only restrain the movement of ceramic fragments but also prevent the peeling off of the adjacent undamaged ceramic tiles. Therefore, Type C targets performed better than B.

Fig. 7 compared the post-ballistic photos for the three targets. The post-ballistic situations of both Type A and B were more or less the same: the different elongations at breaks of ceramic and metal caused the peeling off of adjacent undamaged ceramic tiles from the back plate, implying that the system collapsed after one single shot. It was noting that for Type B targets, the adjacent ceramic tiles around the impact region were not defeated during the impact, but dropped from

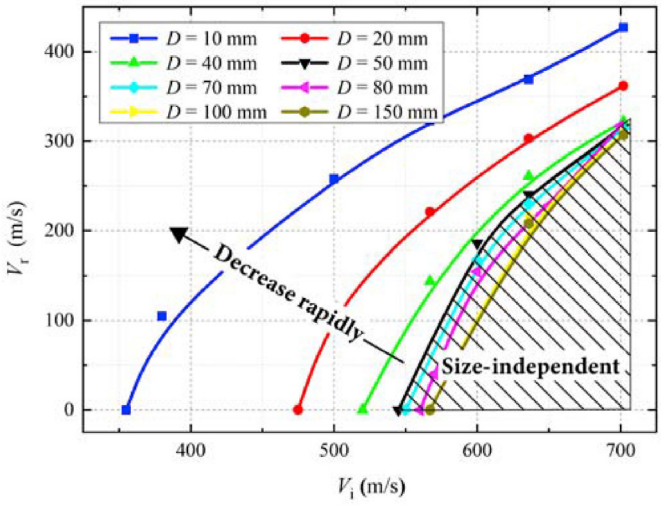

Fig. 8. The ballistic performace of individual ceramic tile with different dimensions.

the backing plate together with the tiles near the boundaries in the subsequent structural response. However, for Type C targets, only the impacted ceramic tile was penetrated by the projectile, while the other tiles remained intact and stayed in the original positions. The presence of the honeycomb lattice preserved the structural integrity of the panels after the single ballistic impact, so that a high degree of residual ballistic resistance remained even after one single impact. This would be expected to enhance the impact resistance against the multiple ballistic impacts.

It could be found from the tests that, only the enhanced mosaic armor (Type C) could efficiently localize the damage region while simultaneously maintain the effective bonding between adjacent tiles and the back plate. The BLV of the Type C target was about 50 ms^{-1} lower than that of Type A, which could be understood as a consequence of the small ceramic tile [20]. For better ballistic resistance and comprehending the penetration mechanism of mosaic amour intuitively and thoroughly, the numerical method was proposed in Section 3.

3. Numerical simulation

3.1. Problem description

To explore the ballistic performance of a bi-layer mosaic armor system against the impact of a blunt projectile, the FE analysis included two main steps:

(1) In the first step, a numerical study was made to establish a connection between ceramic tile size and efficacy of protection.
(2) In the second step, impact locations varying systematically along two different paths, i.e., the central-seam-central (CSC) path and the central-joint-central (CJC) path as shown in Fig. 10, were considered to evaluate the worst case scenario of the armor performance.

3.2. Finite element model

Full 3D model for each armor type was constructed by employing the commercial software LS-DYNA. The back plate was meshed using element SOLID 164 based upon the Lagrangian algorithm. The SPH method was used to model the flat projectile and the central ceramic tiles, since the erosion or deletion of finite elements could cause numerical instability during the complex contact process. To ensure the convergence of the present numerical solutions, the back plate was meshed with element size 0.5 mm, and the size of SPH particles was also set to 0.5 mm for both the central ceramic tile (i.e., the one being directly hit) and the projectile. Both the AISI 4340 steel and aluminum alloy 6061-T6 were modeled using the Johnson-Cook material model, with relevant material and failure constants listed in Table 2. For the ceramic (AD995 alumina) tiles, the Johnson-Holmquist-2 constitutive relation and damage criterion were adopted, with relevant parameters obtained from Ref. [32], as listed in Table 3.

3.3. Discussions

To validate the FE model for the three target types considered in the present study, the numerical simulation results were compared with the experimental measurements. Fig. 3 plotted the projectile residual velocity as a function of its initial velocity impacting the target plate, while numerical and experimental results and the quantitative comparison was given in Table 1. As shown in Fig. 3, the numerical and experimental data agreed well. For three different target types, the experimental and numerical BLV were similar. While for the residual velocity of projectile, the percentage errors of the numerical simulations were found within 10%, and the deviations were less than 30 m/s in absolute value. Overall, good agreement was achieved for each armor type, thus demonstrating the feasibility of the present FE simulations.

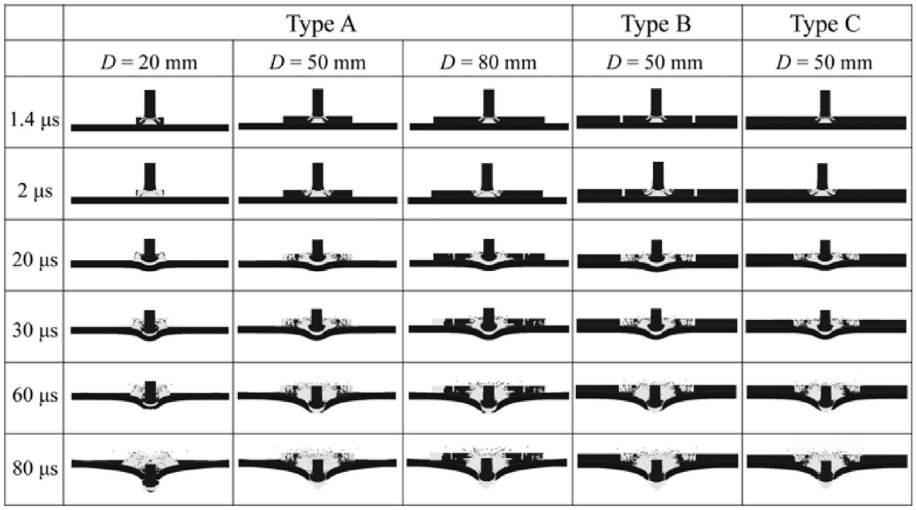

Fig. 9. Numerically simulated damage evolution in Type A, B and C armors at projectile impact velocity of 600 m/s.

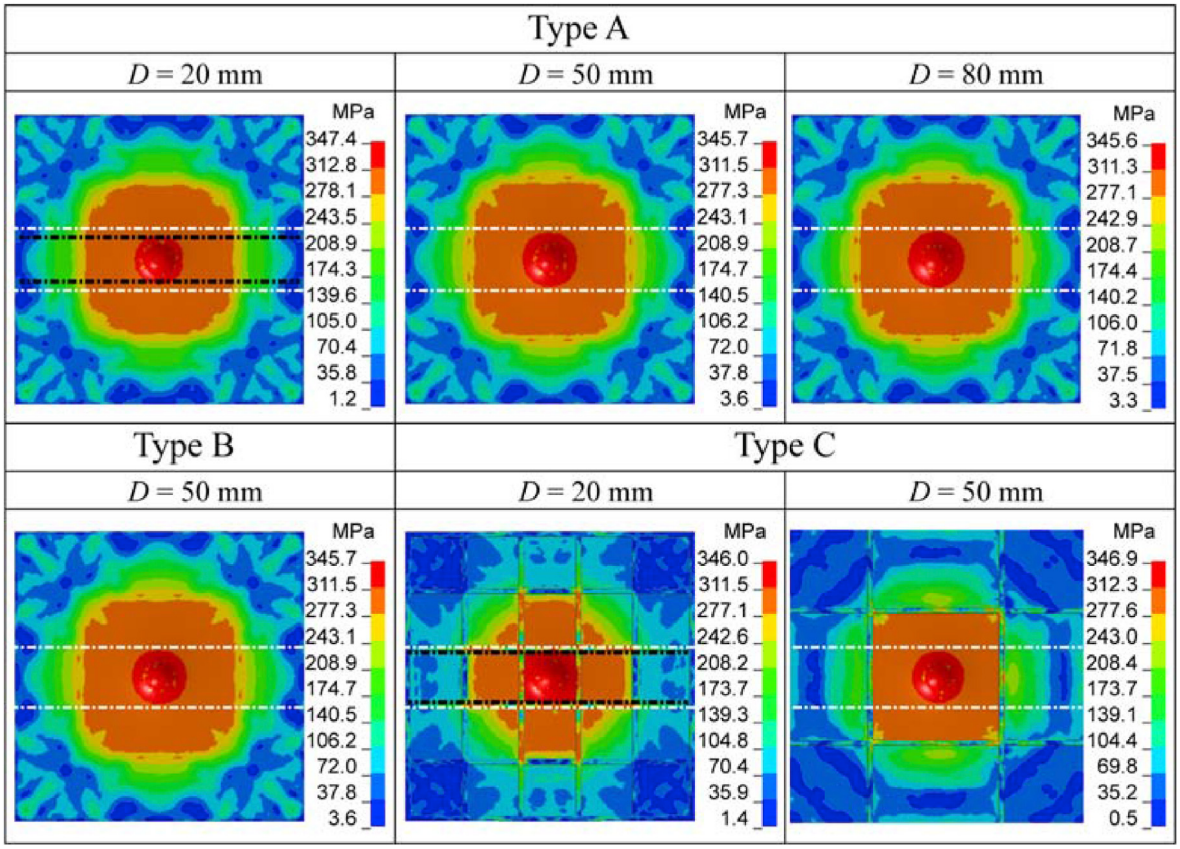

Fig. 10. Numerically simulated stress distributions of back plates in Type A, B and C armors at projectile impact velocity of 600 m/s.

3.3.1. Ceramic tile size

To explore the effect of tile width on ballistic performance, Fig. 8 presented the simulated results for Type A armors subjected to projectile impact at the center, with the tile width systematically decreasing from 150 mm to 10 mm. There existed a critical tile width (about 50 mm): for tile widths exceeding 50 mm, the ballistic performance was more or less insensitive to the tile width; for tile widths less than 50 mm, decreasing the tile width led to a rapidly decrease in ballistic resistance. This explained the drop-off of ballistic performance for Type C armor relative to Type A, as shown in Fig. 3, i.e., the ballistic performance of Type C armor with a ceramic tile width of 20 mm was much weaker than that of Type A armor with a tile width exceeding 100 mm. Therefore, for ceramic/metal bi-layer mosaic armors, ceramic tiles of width 50 mm are recommended.

Fig. 9 compared the numerically simulated damage contours of Type A, B and C armors, with the impact velocity fixed at 600 m/s. For Type A, the ceramic tile width was varied from 20 mm to 80 mm, while it was fixed at 50 mm for Type B and C. For all the three armor types, after the initial impact contact between the projectile and the target, the stress waves were reflected from the ceramic-metal interface, causing a reversed cone-shape damage region for the ceramic tile. For Type A with a tile width of 20 mm, a large amount of ceramic material beneath the projectile moved towards in-plane and out-of-plane directions due to the lack of lateral confinement; on the other hand, the limited tile size of the ceramic material restricted the extension of the cone, thus the impact area of the backing plate was reduced, resulting in the worst performance among the cases studied. However, the ballistic performance of Type A armors could be significantly improved by increasing the tile width to 50 mm or 80 mm, due mainly to the increased flow of ceramic debris against the projectile and the presence of stronger lateral constraints. It should be noted that the conoid of damaged material were similar, and cracks caused by high tensile stress were found at the edge of each Type A target, indicating that the damage had extended to the entire ceramic.

The equivalent stress distributions of back plates in the simulation were also compared in Fig. 10. For Type A with a tile width of 20 mm, the stress was concentrated in the central area (within black lines). By increasing the tile width to 50 mm or 80 mm, the region of the stress concentration extended to a much larger area (within white lines), which implied the more energy dissipation by the back plate. Therefore, a larger tile width usually led to a better ballistic resistance. Comparing with Type A with the tile width of 20 mm, Type C with the same tile width had slightly increased the stress distribution area, mainly attributed to the enhancement of the honeycomb lattice. For Type A, B and C with the tile width of 50 mm, the stress distribution was almost the same. This meant that the contribution of the honeycomb lattice as a lateral restraint frame decreased with the increase of the ceramic tile width. The maximum stresses on the back plate of different target types were similar through the dissipation action of ceramic tiles in the simulation. The results coincided with the ballistic performance and damage evolution results presented in Figs. 8 and 9. As for the back plate in bi-layer armor, the stress distribution revealed the influence of tile width and the enhancement of honeycomb lattice on ballistic performance.

3.3.2. Impact position

Additional numerical simulations were carried out to explore the heterogeneity in ballistic performance when the bi-layer was impacted at different positions. Figs. 11 and 12 presented the variation of residual projectile velocity with varying impact positions for monolithic ceramic targets (Type A) and mosaic ceramic targets (both Type B and C), respectively, with the initial impact velocity increasing from 600 m/s to 900 m/s. It was seen that, for all the three armor types, the ballistic performance was highly dependent on impact position.

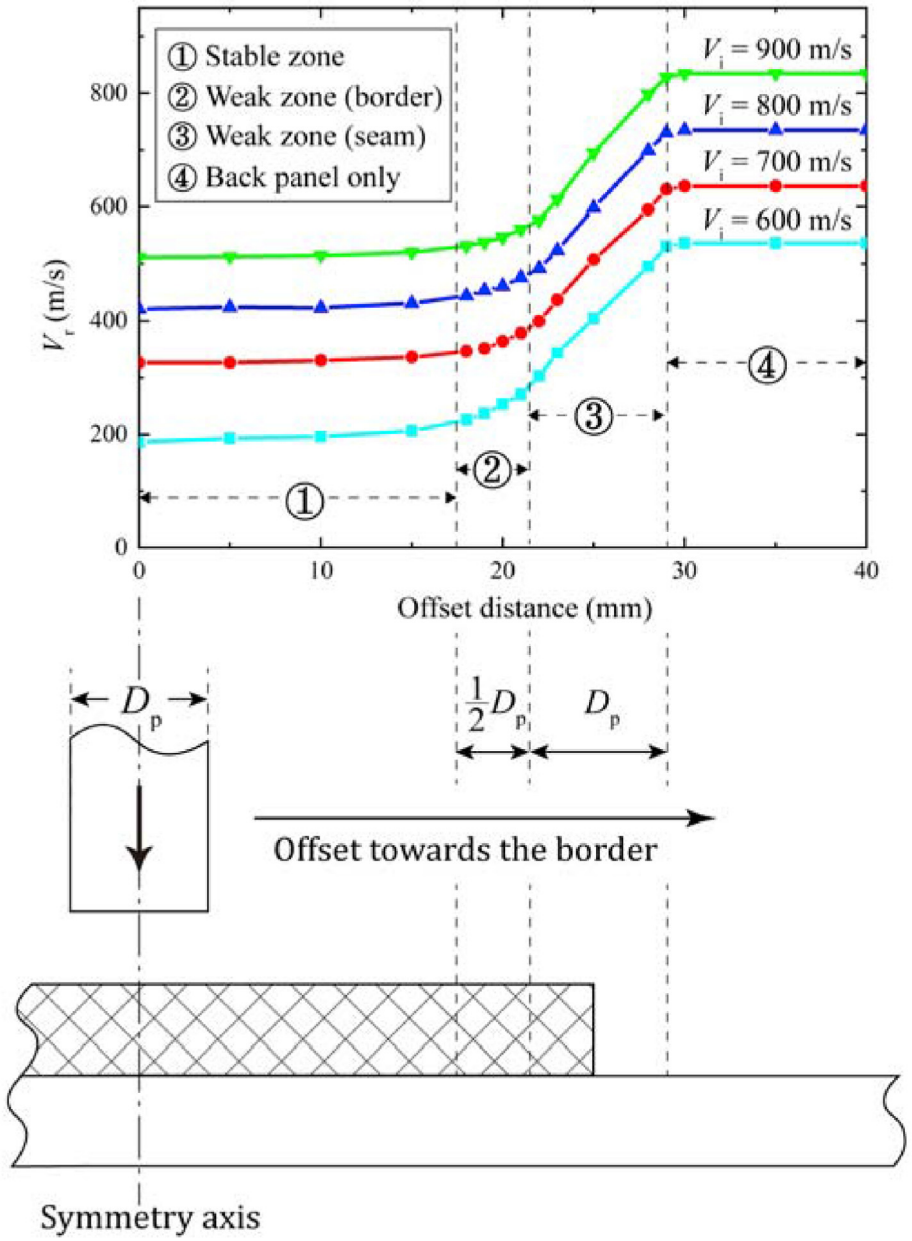

Fig. 11. Residual velocity plotted as a function of impacting position (moving from center to border) for Type A armor.

For Type A armor as shown in Fig. 11, as the impact position was moved to the border, the ballistic performance of the ceramic tile directly hit by the projectile at different velocities exhibited the same variation trend. The residual velocity of projectile (RVP) versus impact position curves could be divided into four regions: in Region 1, the RVP remained almost constant as the impact position was moved away from the center of the armor; in Regions 2 and 3, the RVP increased sharply with increasing offset distance of the impact position, which corresponded to weakened ballistic resistance; in Region 4 (i.e., near the border), the projectile directly impacted the metal backing plate instead of the ceramic tile. It was noticed that the ballistic mechanisms occurring in Region 2 were different from those in Region 3. In Region 2, the dominant mechanism for the weakened ballistic performance could be called the "border effect", which was mainly attributed to the decrease of lateral confinement at the edge of ceramic tile (i.e., the in-plane movement of ceramic fragments led to lower pressures in the vicinity of the impacting projectile). In contrast, the main reason for the weakened performance observed in Region 3 was the gradual decrease of the amount of ceramic material beneath the impact point.

For mosaic armors (*i.e.*, Type B and Type C), the impact position of the projectile (at an initial velocity of 600 m/s) was systematically varied from the center of one ceramic tile to that of the adjacent tile along the path CSC (or CJC), as illustrated in Fig. 12a. It could be seen from the results presented in Fig. 12b that for both armor types, the RVP exhibited a symmetric variation due to the geometric symmetry of the CSC and CJC paths: the RVP for the case impacting in the central region is lower than that for the case impacting in the gap region, meaning that the ballistic resistance of the gap region is weaker than that of the central region. For a mosaic armor, its RVP versus offset distance curve could be divided into three regions: in Regions I and III, the residual velocity increased gradually when the impact position moved away from the tile center for both Type B and C armors, due to the border effect; Region II reflected the ballistic performance when the impact occurred in the gap region. For Type B, impacting in the gap region led to worst ballistic resistance (corresponding to highest residual velocity). However, for the Type C armor, the weakest impact

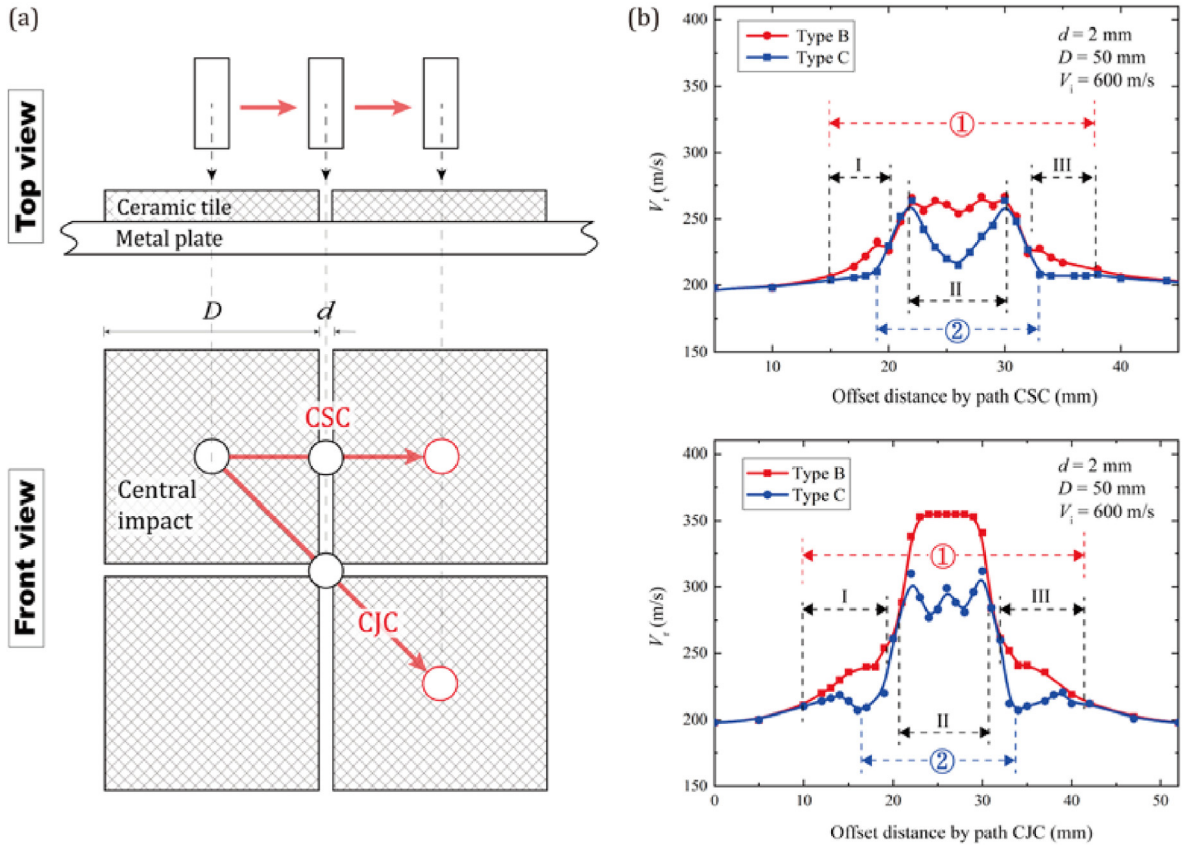

Fig. 12. (a) Schematic of projectile impact position moving along two different paths, CSC and CJC. (b) Variation of residual velocity along projectile impacting path CSC and CJC for Type B and C armors.

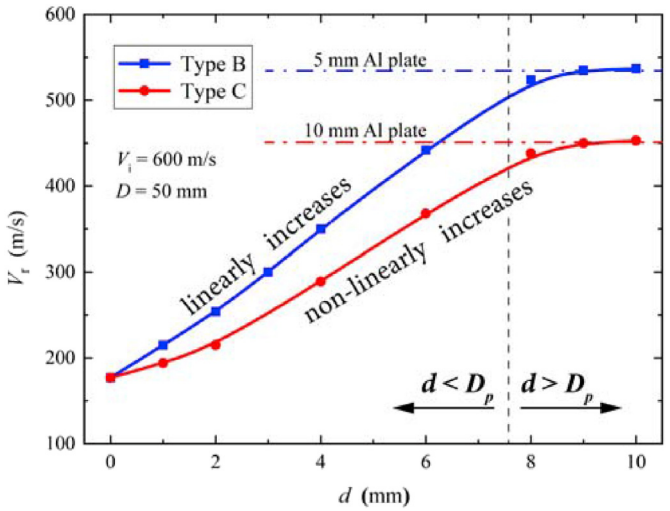

Fig. 13. Residual projectile velocity plotted as a function of inter ceramic tile gap width when impacted at the mid-point of path CSC (Fig. 12a).

position was at a distance 4 mm (approximately equal to the diameter of the projectile D_p) from inter tile gap rather than the center of the gap region, due to the presence of metallic honeycomb webs. Yet due to the enhancement of honeycomb webs (which could be viewed as a gap-filling material and also a lateral restraint frame), the ballistic resistance of Type C impacted in the gap region was superior to that of Type B impacted at the same position, especially at the mid-point of path CJC. Overall, it could be concluded that assessing the ballistic resistance of a bi-layer armor by only considering its performance when impacted at the center of ceramic tile was irrational. It was noticed that the employment of honeycomb lattice also improved the homogeneity of the protective performance of Type C armor impacted at different positions.

3.3.3. Inter tile gap width

When impacted at the mid-point of path CSC (Fig. 12), the dependence of RVP on the gap width between adjacent ceramic tiles, *d*, was presented in Fig. 13. To this end, the width of ceramic tiles was fixed at 50 mm, while the initial projectile impact velocity was 600 m/s. It could be expected that a larger *d* would lead to the increase of RVP. For type B armors, an enlarged gap meant that the amount of ceramic material beneath the impact point decreased. Therefore, the computational results demonstrated an inverse linear relation between the RVP and inter tile gap width. While for type C, on one hand, due to the combined effect of lateral restraint and filling material, the variation of RVP underwent a non-linear process; on the other hand, the ballistic performance was improved relative to Type B. For Type B and C armors with a gap width *d* larger than D_p, the ballistic performance was independent of *d* and was equivalent to that of monolithic aluminum plate of thickness 5 mm and 10 mm, respectively, as shown in Fig. 13.

3.4. Performance evaluation under multiple impacts

For practical applications, the armor is often required to resist multiple projectile impacts launched by, e.g., automatic weapons. So a qualified ceramic/metal bi-layer armor must be demonstrated that a single projectile impact on one ceramic tile did not affect significantly the performance of adjacent tiles upon subsequent impact(s). Based upon the analysis presented in Section 2, for the three armor types studied here, only the proposed honeycomb enhanced mosaic armor could meet the requirements. With single-shot ballistic data explored in section 3.3, the multi-hit ballistic resistance could be defined

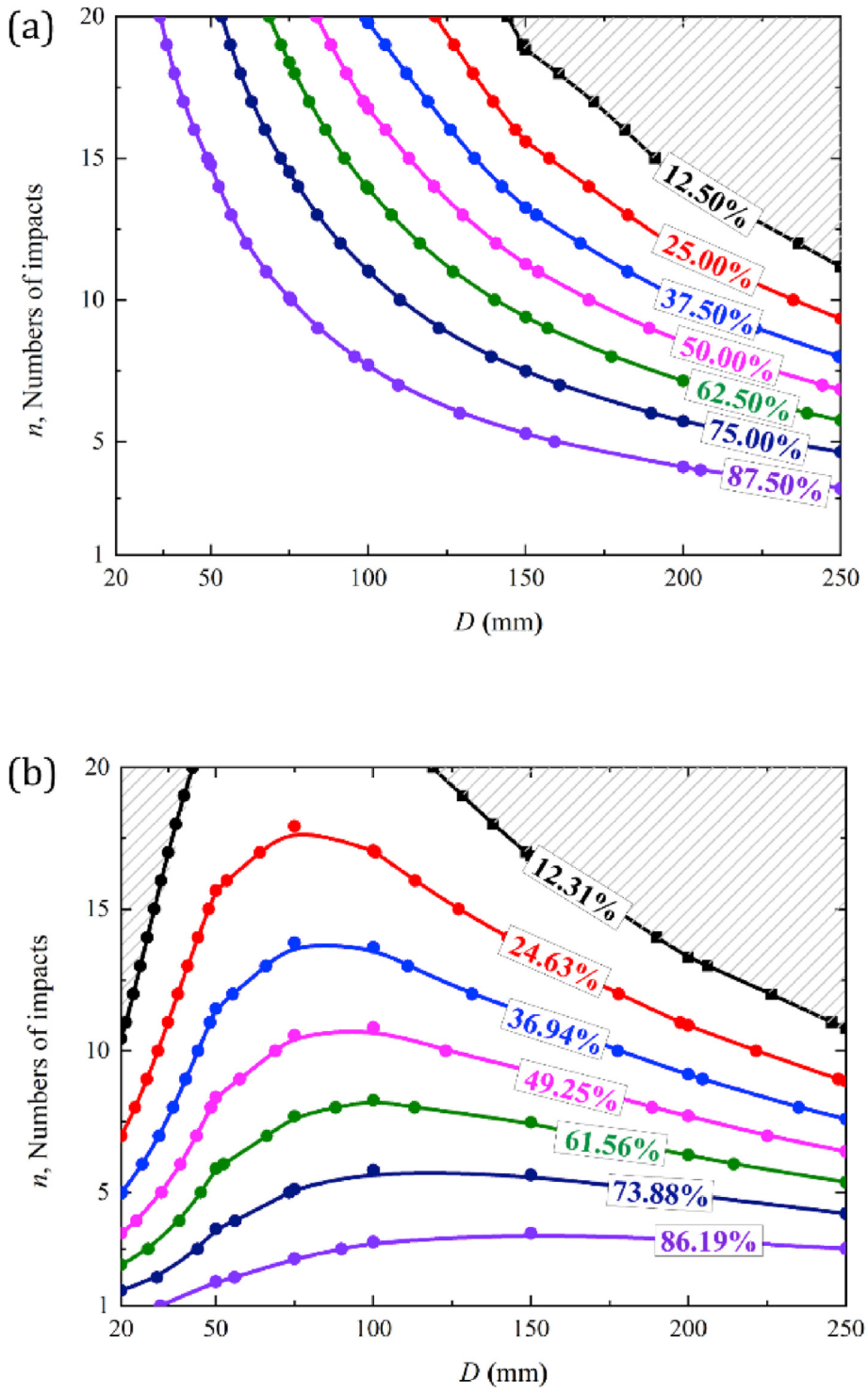

Fig. 14. Probability contour of ceramic/metal bi-layer mosaic armor which could defeat n rounds of projectile impact (a) armor with no weak zone (i.e., $\Delta = 0$): and (b) armor with 1 mm wide weak zone (i.e., $\Delta = 1$mm).

statistically and the probability of target defeating rounds studied, as demonstrated below.

3.5. Basic methodology

The basic methodology adopted was similar to that of de Rosset [35], except that the effect of inter tile gap width was accounted for. The simplifying assumptions made to develop the methodology include: (1) The impact locations could be described with a uniform random distribution; (2) The tile geometry was taken as a square with side length D; (3) The hit on one ceramic tile left adjacent ceramic tiles unaffected; (4) One tile could defeat one impact only; (5) Zone of weak performance had a width of Δ; (6) The projectile could impact only one tile at a time; (7) let A be an area that contained the hit locations of n rounds, and the tile size was small in comparison to A, i.e., $A = N(D + d/2)^2$, N being the number of tiles contained within A.

The probability that the first round in the burst was defeated by the armor was given by:

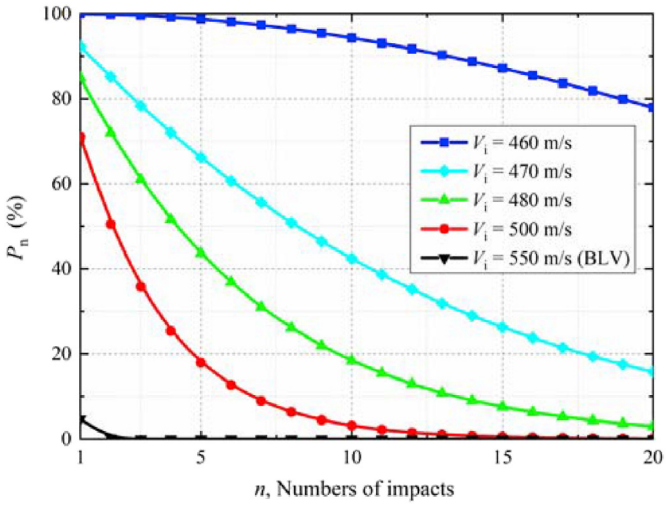

Fig. 15. Multiple impact capability of Type C armor at different impact velocities.

$$P_1 = [1 - \Delta/(D + d/2)]^2 \quad (1)$$

After the first impact, one ceramic tile had been destroyed, and the probability that the mosaic armor defeated two rounds was given by:

$$P_2 = [(N - 1)/N][1 - \Delta/(D + d/2)]^4 \quad (2)$$

Similarly, the probabilityP_n that the armor defeated n rounds was given by:

$$P_n = \left[\frac{N!}{N^n(N-n)!}\right]\left[1 - \frac{\Delta}{(D + d/2)}\right]^{2n} \quad (3)$$

For maximum armor performance, both N and $D + d/2$ needed to be as large as possible. Further, given that $A = N(D + d/2)^2$, N and $D + d/2$ were a pair of opposite quantities.

For $\Delta = 0$, as shown in Fig. 14a, the results dictated that ceramic tiles adopted by a mosaic armor should be as small as possible (i.e., large N) for maximum armor performance. However, there existed practical limits. If the tiles were too small, the size effect would greatly affect the ballistic performance, as discussed in detail in Section 3.3. Thus even for a mosaic armor without zones of weak performance, there was a critical tile size. For the comparison model $\Delta = 1$ as shown in Fig. 14b, to defeat 5 rounds, the tile size should be about 100 mm. To defeat 15 or 20 rounds, however, 75 mm was a better choice. The results indicated that there existed an optimal size of ceramic tiles that depended upon the defeats rounds (n). By considering the number of impacts and weak zone area as additional influencing factors, this methodology enabled balancing ceramic tile size and protection requirements in a comprehensive manner.

3.6. Reliability calculation

For the proposed honeycomb enhanced mosaic armor, the methodology was also used to determine its ballistic performance under different projectile impact velocities during multi-hitting events.

With the ceramic tile size fixed at $D = 50$ mm, the weak zone width Δ changed with different threat levels. When the impact velocity was 550 m/s (the BLV under single central impact), the practical weak zone width $\Delta = 19$ mm. While for an impact velocity of 460 m/s, the practical weak zone width $\Delta = 0$ mm. For illustration, with $A = 2$ m^2 assumed, the calculated values of P_n versus n were presented in Fig. 15 for Type C armor subjected to different initial projectile impact velocities.

With the results of Fig. 15, it was straightforward to show how these impact velocities would affect the value of P_n, the probability of non-perforation through the n-th projectile impact. When the Type C armor was impacted at the single central BLV (550 m/s), although the armor could defeat the impact as observed in the experiment, according to the corresponding value of P_n shown in Fig. 15, its multi-hit capability was very poor, even after the very first impact. With decreasing impact velocity, the armor's multiple impact capability gradually increased, and a critical velocity of 460 m/s emerged. When the impact velocity was below or equaled to this critical velocity, the armor behaved like one with no weak zone (i.e., similar to that of Fig. 15a). These results indicated that armor designs needed to consider the trade-off between (1) ceramic tiles which had a high BLV but single impact capability only, and (2) tiles with lower BLV but multiple impact capability.

4. Conclusions

A combined experimental and numerical approach was employed to investigate the ballistic performance of ceramic/metal bi-layer mosaic armors. The influences of ceramic tile size, impact position, border-effect and inter tile gap width on ballistic performance were systematically explored. The performance of honeycomb enhanced mosaic armor under multiple impacting was also evaluated. Main conclusions are summarized as follows:

(1) Compared with monolithic ceramic armor, the traditional mosaic armor could limit the damage region but the bonding between ceramic and the back plate was weak after projectile impact. Only the proposed honeycomb enhanced mosaic armor could efficiently localize the damage region and maintain effective bonding between adjacent tiles and the back plate. In other words, the proposed mosaic armor enables balanced single and multiple impact resistance.
(2) A critical dimension of ceramic tiles existed under single central impact. For the configurations considered, the minimum tile size was about 50 mm. When the tile size was larger than the critical one, honeycomb lattice enhancement could maintain effective ceramic-metal bonding and keep the undamaged ceramic tiles in place.
(3) High dependency of residual projectile velocity on impact position was observed, both in the traditional mosaic armor and the honeycomb enhanced mosaic armor. However, due to the enhancement of metallic lattice, the honeycomb enhanced armor exhibited a greatly reduced weak zone compared to the traditional mosaic armor. Meanwhile, as a result of honeycomb enhancement, the distribution of weak zone had also been changed: the weakest impact position of the armor was not at the center of the gap or joint, but at a certain distance from the border.
(4) With the extended reliability calculation method, it was demonstrated that single shot ballistic data could be used to estimate armor performance against multiple projectile impacts. Under multiple projectile impacts, the single central impact BLV could not represent the ballistic resistance of armors.

CRediT authorship contribution statement

Zhong-Nan Zhao: Conceptualization, Methodology, Software, Validation, Formal analysis, Investigation, Data curation, Writing - original draft, Writing - review & editing, Visualization. **Bin Han:** Resources, Writing - review & editing, Supervision, Project administration. **Fei-Hao Li:** Software, Validation. **Rui Zhang:** Software. **Peng-Bo Su:** Validation. **Mao Yang:** Validation. **Qi Zhang:** Resources. **Qian-Cheng Zhang:** Resources. **Tian Jian Lu:** Resources, Writing - review & editing, Supervision, Project administration, Funding acquisition.

Acknowledgments

This work was supported by the National Natural Science

Foundation of China (11902148, 11802221, 11972185 and 51875441), the National Key R&D Program of China (2018YFB1106400), the China Postdoctoral Science Foundation (2016M600782), the Postdoctoral Scientific Research Project of Shaanxi Province (2016BSHYDZZ18), the Zhejiang Provincial Natural Science Foundation of China (LGG18A020001), the Natural Science Basic Research Plan in Shaanxi Province of China (2018JQ1078), the Natural Science Fund Project in Jiangsu Province of China (BK20190392), the State Key Laboratory of Smart Manufacturing for Special Vehicles and Transmission System + GZ2019KF015, and the Open Fund of the State Key Laboratory of Mechanics and Control of Mechanical Structures (Nanjing University of Aeronautics and astronautics, MCMS-I-0219K01 and MCMS-E0219K02).

References

[1] M.L. Wilkins, Mechanics of penetration and perforation, Int. J. Eng. Sci. 16 (1978) 793–807.
[2] D. Sherman, T. Ben-Shushan, Quasi-static impact damage in confined ceramic tiles, Int. J. Impact Eng. 21 (1998) 245–265.
[3] P.J. Hazell, N.A. Fellows, J.G. Hetherington, A note on the behind armour effects from perforated alumina/aluminium targets, Int. J. Impact Eng. 21 (1998) 589–595.
[4] C.Y. Ni, Y.C. Li, F.X. Xin, F. Jin, T.J. Lu, Ballistic resistance of hybrid-cored sandwich plates: numerical and experimental assessment, Compos. Appl. Sci. Manuf. 46 (2013) 69–79.
[5] R. Chi, A. Serjouei, I. Sridhar, G.E.B. Tan, Ballistic impact on bi-layer alumina/aluminium armor: a semi-analytical approach, Int. J. Impact Eng. 52 (2013) 37–46.
[6] F. Bouville, E. Maire, S. Meille, B. Van de Moortèle, A.J. Stevenson, S. Deville, Strong, tough and stiff bioinspired ceramics from brittle constituents, Nat. Mater. 13 (2014) 508–514.
[7] Z. Liu, M.A. Meyers, Z. Zhang, R.O. Ritchie, Functional gradients and heterogeneities in biological materials: design principles, functions, and bioinspired applications, Prog. Mater. Sci. 88 (2017) 467–498.
[8] H. Wu, G. Fan, An overview of tailoring strain delocalization for strength-ductility synergy, Prog. Mater. Sci. 113 (2020) 100675.
[9] W.S. de Rosset, J.K. Wald, Analysis of Multiple-Hit Criterion for Ceramic Armor, US Army Laboratory technical report, 2003, p. 2861.
[10] M. Grujicic, B. Pandurangan, B. d'Entremont, The role of adhesive in the ballistic/structural performance of ceramic/polymer–matrix composite hybrid armor, Mater. Des. 41 (2012) 380–393.
[11] E. Medvedovski, Ballistic performance of armour ceramics: influence of design and structure. Part 2, Ceram. Int. 36 (2010) 2117–2127.
[12] S.J. Bless, D.L. Jurick, Design for multi-hit capability, Int. J. Impact Eng. 21 (1998) 905–908.
[13] R. Zaera, S. Sánchez-Sáez, J.L. Pérez-Castellanos, C. Navarro, Modelling of the adhesive layer in mixed ceramic/metal armours subjected to impact, Compos. Appl. Sci. Manuf. 31 (2000) 823–833.
[14] M. Übeyli, R.O. Yıldırım, B. Ögel, Investigation on the ballistic behavior of Al2O3/Al2024 laminated composites, J. Mater. Process. Technol. 196 (2008) 356–364.
[15] R. Goel, M.D. Kulkarni, K.S. Pandya, N.K. Naik, Stress wave micro–macro attenuation in ceramic plates made of tiles during ballistic impact, Int. J. Mech. Sci. 83 (2014) 30–37.
[16] W. Seifert, E. Strassburger, S. Grefen, S. Schaare, Experimental study about the influence of adhesive stiffness to the bonding strengths of adhesives for ceramic/metal targets, Defence Technol. 12 (2016) 188–200.
[17] C.E. Anderson, S.A. Royal-Timmons, Ballistic performance of confined 99.5%-Al203 ceramic tiles, Int. J. Impact Eng. 19 (1997) 703–713.
[18] J. López-Puente, A. Arias, R. Zaera, C. Navarro, The effect of the thickness of the adhesive layer on the ballistic limit of ceramic/metal armours. An experimental and numerical study, Int. J. Impact Eng. 32 (2005) 321–336.
[19] A. Harris, B. Vaughan, J. Yeomans, P. Smith, S. Burnage, Ballistic testing of surface-treated alumina and silicon carbide with improved adhesive bond strength, Int. J. Appl. Ceram. Technol. 14 (2017) 323–330 Wiley Periodicals, Inc. on behalf of American Ceramics Society (ACERS).
[20] P.J. Hazell, C.J. Roberson, M. Moutinho, The design of mosaic armour: the influence of tile size on ballistic performance, Mater. Des. 29 (2008) 1497–1503.
[21] W. Seifert, E. Strassburger, M. Dolak, S. Schaare, Experimental study on the dependency of the ballistic performance of tiled ceramic/metal targets on inter tile gap width and projectile impact position, Int. J. Impact Eng. 122 (2018) 50–59.
[22] Z. Shen, D. Hu, G. Yang, X. Han, Ballistic reliability study on SiC/UHMWPE composite armor against armor-piercing bullet, Compos. Struct. 213 (2019) 209–219.
[23] K. Dasgupta, Role of carbon nanotubes in the ballistic properties of boron carbide/carbon nanotube/ultrahigh molecular weight polyethylene composite armor, Ceram. Int. 46 (2020) 4137–4141.
[24] Q. Wang, Z. Chen, Z. Chen, Design and characteristics of hybrid composite armor subjected to projectile impact, Mater. Des. 46 (2013) 634–639.
[25] Z. Yin, J. Yuan, M. Chen, D. Si, C. Xu, Mechanical property and ballistic resistance of graphene platelets/B4C ceramic armor prepared by spark plasma sintering, Ceram. Int. 45 (2019) 23781–23787.
[26] J. Jiusti, E.H. Kammer, L. Neckel, N.J. Lóh, W. Trindade, A.O. Silva, O.R.K. Montedo, A. De Noni, Ballistic performance of Al2O3 mosaic armors with gap-filling materials, Ceram. Int. 43 (2) (2017) 2697–2704.
[27] B. Han, Z.-J. Zhang, Q.-C. Zhang, Q. Zhang, T.J. Lu, B.-H. Lu, Recent advances in hybrid lattice-cored sandwiches for enhanced multifunctional performance, Extreme Mech. Lett. 10 (2017) 58–69.
[28] C. Ni, R. Hou, B. Han, F. Jin, G. Ma, T. Lu, Normal and oblique projectile impact of double-layered pyramidal lattice truss structures filled with ceramic insertions, J. Thermoplast. Compos. Mater. 30 (2017) 1136–1156.
[29] M. Yang, B. Han, P.-B. Su, Z.-H. Wei, Q. Zhang, Q.-C. Zhang, T.J. Lu, Free vibration and axial compression of all-metallic cylindrical and truncated conical sandwich shells with corrugated cores, J. Sandw. Struct. Mater. (2020) Epub ahead of print.
[30] L.L. Yan, B. Yu, B.a. Han, Q.C. Zhang, T.J. Lu, B.H. Lu, Effects of aluminum foam filling on the low-velocity impact response of sandwich panels with corrugated cores, J. Sandw. Struct. Mater. 22 (2020) 929–947.
[31] D.A. Shockey, A.H. Marchand, S.R. Skaggs, G.E. Cort, M.W. Burkett, R. Parker, Failure phenomenology of confined ceramic targets and impacting rods, Int. J. Impact Eng. 9 (1990) 263–275.
[32] R. Krashanitsa, S. Shkarayev, Computational study of dynamic response and flow behavior of damaged ceramics, 46th AIAA/ASME/ASCE/AHS/ASC Structures, Structural Dynamics and Materials Conference, American Institute of Aeronautics and Astronautics, Austin, Texas, 2005.
[33] G.R. Johnson, W.H. Cook, Fracture characteristics OF 3 metals subjected to various strains, strain rates, temperatures and pressures, Eng. Fract. Mech. 21 (1985) 31–48.
[34] F. Hajializadeh, M.M. Mashhadi, Investigation and numerical analysis of impulsive hydroforming of aluminum 6061-T6 tube, J. Manuf. Process. 20 (2015) 257–273.
[35] W.S. de Rosset, Patterned armor performance evaluation, Int. J. Impact Eng. 31 (2005) 1223–1234.